Journal of Inorganic and Organometallic Polymers and Materials (2024) 34:745–758
https://doi.org/10.1007/s10904-023-02857-9

RESEARCH

# Preparation of Composite Porous Hydrogel Montmorillonite/Humic Acid/Polyvinyl Alcohol@Polypyrrole Based on Pickering Emulsion Template Method for Enhancing Hexavalent Chromium Ions Adsorption from Aqueous Solution

**Xuejiao Zhang[1] · Yulin Li[1] · Wenjie Zou[1] · Li Ding[1] · Jun Chen[1]**

Received: 28 May 2023 / Accepted: 2 September 2023 / Published online: 20 September 2023


**Abstract**
Polypyrrole (PPy) is a typical conductive polymer, which has certain adsorption capacity for Cr(VI). However, it is easy to agglomerate during polymerization, and its adsorption capacity cannot be fully exerted due to the reduction of adsorption sites and specific surface area. In this work, a novel composite porous hydrogel adsorbent montmorillonite/humic acid/polyvinyl alcohol@polypyrrole (MMT/HA/PVA@PPy) was successfully prepared by Pickering emulsion template-in-situ chemical oxidative polymerization, which gave full play to the potential adsorption efficiency of PPy for Cr(VI). The results of Fourier transform infrared spectroscopy (FTIR), elemental analysis (EDX) and field emission scanning electron microscopy (FESEM) confirmed that PPy was successfully compounded with MMT/HA/PVA, and PPy was evenly distributed on the composite. The adsorption experiment results show that the optimal adsorption capacity of MMT/HA/PVA@PPy composite for Cr(VI) reaches 106.29 mg/g at 318 K. The adsorption mechanism analysis suggested that the Cr(VI) removal may be mainly related with ion exchange, electrostatic interaction and redox. MMT/HA/PVA@PPy is a useful adsorbent for removing Cr(VI) ions, which provides an effective way to develop more efficient Cr(VI) ion adsorbent.

**Keywords** Polypyrrole · Hexavalent chromium · Composite porous hydrogel · Pickering emulsion template · Adsorption

## 1 Introduction

Hexavalent chromium Cr(VI) generally exists in the form of chromate ($CrO_4^{2-}$), hydrogen chromate ($HCrO_4^-$), and dichromate ($Cr_2O_7^{2-}$) in wastewater discharged from industries such as electroplating, chromium salt manufacturing, textile printing and dyeing, and metal smelting [1–4]. As we all know, Cr(VI) is harmful to carcinogenicity and gene mutation. Short-term inhalation of high-dose Cr(VI) compounds will cause health problems such as nasal mucosa allergy, perforation and erosion of nasal septum. When ingested in large doses, it will lead to gastric ulcer, kidney and liver damage and even death [5–8]. Treatment of Cr(VI) in water is very important to the environment and human health. Among many technologies for treatment of Cr(VI), adsorption has attracted much attention because of its advantages of simplicity, high efficiency, low cost, no secondary pollution and recycling. Adsorption can also selectively recover useful substances from water by endowing adsorbent with special recognition ability [9–11]. Therefore, adsorption has always been the preferred method to treat Cr(VI) in water.

Adsorption method mainly depends on the performance of adsorption materials, which determines the adsorption efficiency and cost. Polypyrrole (PPy) is a unique adsorption material, which is widely used in wastewater treatment because of its low cost, non-toxicity, stable environment, easy synthesis and good chemical modification possibility [12–14]. There are some positively charged nitrogen atoms in PPy chain, in order to keep the charge neutral, PPy will adsorb anions in aqueous solution through ion exchange and electrostatic interaction, so it has good adsorption capacity for Cr(VI) [15–17]. Many experiments have proved that polypyrrole has good adsorption performance for Cr(VI).

✉ Jun Chen
junchen@ahut.edu.cn

[1] College of Chemistry and Chemical Engineering, Anhui University of Technology, Ma Xiang Road, Ma'anshan 243000, People's Republic of China

Mdlalose et al. [18] prepared polypyrrole/montmorillonite clay flexible composite adsorbent for Cr(VI) adsorption by in situ oxidative polymerization method. Thao et al. [19] synthesized free-standing PPy/PANI composite films by the interfacial polymerization of pyrrole and aniline gaseous monomer at vapor/liquid interface to enhance the adsorption capacity of Cr(VI). However, polypyrrole powder does not show high adsorption capacity due to its lack of porous structure and low surface area [20]. In addition, polypyrrole particles will agglomerate with each other during the π-π stacking process, which makes it difficult for doped anions (such as $Cl^-$) to diffuse from the polymer, thus limiting the removal efficiency of Cr(VI) [21, 22]. Therefore, to give full play to the potential performance of polypyrrole in water treatment, we can start from two aspects: one is to avoid the agglomeration of polypyrrole during the polymerization process. Secondly, polypyrrole composites with porous structure were prepared to increase the specific surface area.

Polymer hydrogel has a hydrophilic three-dimensional network structure, and the existence of functional groups such as –COOH, –OH, $–SO_3H$ and $–CONH_2$ in the network helps to improve its ability to remove heavy metal ions, such as polyacrylic acid, polyvinyl alcohol and Poly (2-acrylamido-2-methylpropanesulfonic acid) [23–25]. The special geometric and physical–chemical properties of polymer hydrogel can provide a uniform system and porous structure for pyrrole polymerization. Emulsion polymerization is one of the ideal strategies to obtain porous hydrogels, but the traditional surfactant-stabilized emulsion often has the disadvantages of foaming, high toxicity and high cost [26]. Pickering emulsion is stabilized by amphiphilic particles, which spontaneously migrate to the oil–water interface and form a rigid shell around the droplets in the internal phase to prevent them from coalescing [27].

Compared with the traditional surfactant-stabilized emulsion, the emulsion stabilized by solid particles has higher interfacial adhesion energy and long-term stability [28, 29]. Pickering emulsion has many advantages, such as strong coalescence resistance, good long-term stability, good biocompatibility and adjustable properties, which make it an excellent template for producing various porous hydrogels [30–32]. It is worth mentioning that the choice of solid particles will directly affect the stability and droplet size of Pickering emulsion [33, 34]. Clay, as a solid particle with colloid size, large reserves and low cost, has great advantages in stabilizing Pickering emulsion. Montmorillonite, as a typical natural clay material, has negative charge (because $Si^{4+}$ and $Al^{3+}$ are replaced by other cations), high surface area and good adsorption, so they have certain adsorption capacity for heavy metal ions [35–37]. The removal efficiency of natural montmorillonite (MMT) is limited. In order to improve the adsorption performance, biomass materials (such as humic acid), metal oxides and cationic surfactants are usually used to modify it [38, 39]. Humic acid (HA) is a kind of natural organic matter widely distributed in nature [40, 41], which contains carbonyl, carboxyl and hydroxyl groups in its molecule, making it have the functions of adsorption and exchange. By replacing inorganic cations in MMT with HA, the cation form and interlayer ion form of MMT crystal layer can be changed, and its adsorption performance for heavy metal ions can be improved [42–44].

Polypyrrole has a high adsorption capacity for Cr(VI) due to its unique ion exchange and redox characteristics. However, the reduction of adsorption sites caused by agglomeration makes it impossible to fully exert its adsorption ability [45–47]. In order to reduce the agglomeration of PPy and increase the exposure of active adsorption sites, so as to give full play to the potential adsorption performance of PPy, a composite porous hydrogel adsorbent of montmorillonite/humic acid/polyvinyl alcohol@polypyrrole (MMT/HA/PVA@PPy) was prepared by Pickering emulsion template in-situ oxidative polymerization. It is expected that hydrogel network and Pickering emulsion template have double "limiting" effects on PPy, which can reduce the agglomeration of PPy, increase the exposure of active adsorption sites and give full play to the potential adsorption performance of PPy. Specifically, oil-in-water Pickering emulsion droplets template were prepared with montmorillonite/humic acid (MMT/HA) composite colloidal particles as stabilizers. The positively charged nitrogen-containing groups in pyrrole and the negatively charged groups at the interface of emulsion droplets would generate electrostatic attraction, so that pyrrole could be oxidized and polymerized in situ at the interface of emulsion droplets. Then, polyvinyl alcohol (PVA) was crosslinked by freeze–thaw cycle method to form a three-dimensional network structure to obtain hydrogel. Finally, MMT/HA/PVA@PPy composite porous hydrogel was obtained by solvent evaporation-freeze drying (Fig. 1). At the same time, the structure of the material was characterized by FESEM, EDX and FTIR, and its adsorption performance for Cr(VI) was investigated through the effects of solution pH, adsorbent dosage, adsorption kinetics and adsorption thermodynamics experiments. The MMT/HA/PVA@PPy composite porous hydrogel prepared in this study to adsorb Cr(VI), which gives full play to the adsorption potential of PPy itself, improves the utilization rate of PPy, and is also in line with the concept of developing environmental-friendly adsorbents. Another is to utilize composite colloidal particles with abundant and low-cost montmorillonite and humic acid to synergistically stabilize Pickering emulsion, which enriches the stabilization methods of Pickering emulsion.

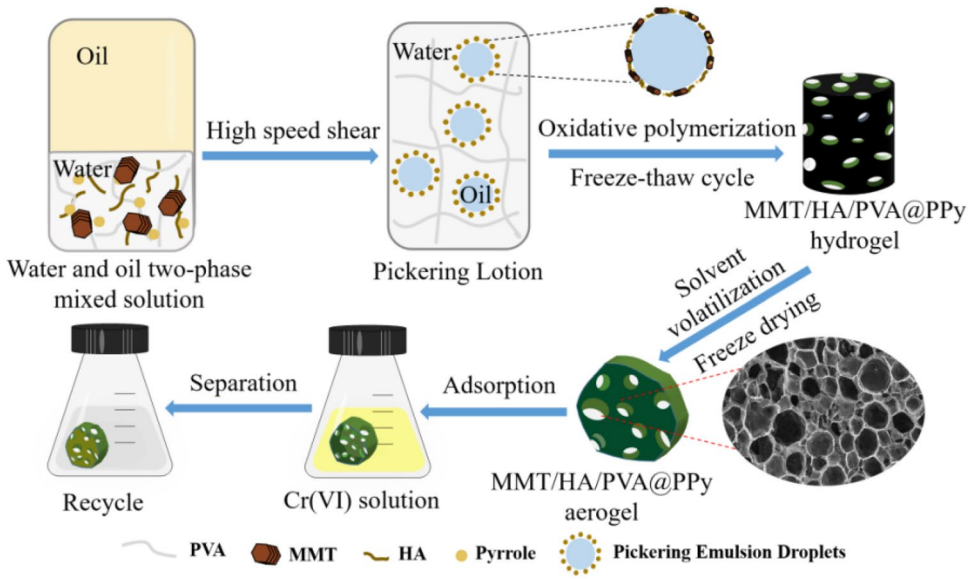


**Fig. 1** Schematic diagram of preparation of MMT/HA/PVA@PPy adsorbent and adsorption of Cr(VI)

## 2 Materials and Methods

### 2.1 Raw Materials

Montmorillonite (MMT) was purchased from Nanocor Company of America. Humic acid (HA) was purchased from Houma Jiayou Humic Acid Co., Ltd. Polyvinyl alcohol (PVA, polymerization degree is about 1700), cyclohexane ($C_6H_{12}$), potassium dichromate ($K_2Cr_2O_7$), pyrrole ($C_4H_5N$), acetone ($C_3H_6O$), 1,5-diphenylcarbazide, phosphoric acid ($H_3PO_4$), sulfuric acid ($H_2SO_4$), ammonium persulfate (APS) ($(NH_4)_2S_2O_8$), hydrochloric acid (HCl), sodium hydroxide (NaOH) and ethanol ($C_2H_6O$) were purchased from Sinopharm Chemical Reagents Co., Ltd. (Shanghai, China). All stock solutions were prepared with deionized water for material preparation and adsorption experiments.

### 2.2 Preparation of MMT/HA/PVA@PPy Adsorbent

0.064 g MMT and 0.0064 g HA were dissolved in 11 g water which had been already adjusted to pH 11, and stirred for 10 min to obtain a uniform MMT/NaHA solution. 3.2 mL hydrochloric acid solution (5 M) was added to obtain MMT/HA composite colloidal particle solution, Then, 16 g of 10% PVA solution and 0.08 g pyrrole were added in turn, and the water phase was obtained by stirring evenly. 61.70 mL cyclohexane as oil phase was poured into water phase under high shear, and a uniform and stable oil-in-water Pickering emulsion was obtained. In addition, 0.28 g ammonium persulfate was dissolved in 4 mL hydrochloric acid solution (0.5 M), poured into the Pickering emulsion, stirred slowly until the color was uniform, and stood for reaction for 12 h. After the polymerization, the hydrogel was obtained by freeze-thaw cycle for five times. Wash with deionized water and ethanol to remove oil phase, unreacted monomers and oligomers. MMT/HA/PVA@PPy composite porous adsorbent was obtained by freeze-drying and stored for later use.

### 2.3 Characterization of MMT/HA/PVA@PPy Adsorbent

Optical microscope (Motic, MOTIC CHINA GROUP CO., LTD) was used to observe the droplet stability of Pickering emulsion and take photos to record the droplet size. The elemental composition and micro-morphology of the materials before and after adsorption were measured by field emission scanning electron microscope (FESEM) equipped with energy dispersion analysis system of X-ray spectrometer (EDX) (NOVA Nano SEM 430, FEI Corporation). Fourier transform infrared spectrometer (FT-IR, PerkinElmer, USA) was used to analyze the functional groups of PPy, MMT/HA/ PVA and MMT/HA/PVA@PPy before and after adsorption. The infrared spectra were recorded in the wave number range of 400–4000 $cm^{-1}$ at room temperature, with a spectral resolution of 4 $cm^{-1}$ and 16 scanning times. The crystal structure changes of the materials was determined by X-ray diffraction (XRD, Bruker D8ADVANCE) in the range of 1–10 (2θ) with (Cu Ka radiation (1.54 Å)) operated. The X-ray photoelectron spectroscopy (XPS) of MMT/HA/PVA@PPy before and after adsorption were studied by ESCALAB 250XI Xray photoelectron spectrometer (Thermo Fisher) with Al Kα radiation (1486.6 eV). Ultraviolet-visible spectro-photometer (UV3600, Shimadzu Corporation) was used to evaluate the adsorption capacity of MMT/HA/PVA@PPy for Cr(VI) in the wavelength range of 500–700 nm.

### 2.4 Batch Adsorption Experiments

A series of adsorption tests of Cr(VI) on MMT/HA/PVA@PPy composites were carried out to analyze the effects of pH value of solution, dosage of adsorbent, reaction time, initial concentration and temperature of Cr(VI) solution on the adsorption performance of the materials. The diluted $K_2Cr_2O_7$ stock solution (1000 mg/L) was used to prepare Cr(VI) solutions with different concentrations, and the pH was adjusted by adding HCl or NaOH solution. In the range of pH 2–10, 0.01 g MMT/HA/PVA@PPy was added into 10 mL Cr(VI) solution with a concentration of 100 mg/L, and the solution was shaken at 298 K for 12 h to study the effect of pH value on adsorption performance. In the dosing experiment, 0.005–0.05 g of adsorption materials were added to the initial concentration of Cr(VI) solution of 100 mg/L, and the pH of the solution was adjusted to 2, and the solution was shaken at 298 K for 12 h. Thermodynamic experiment was carried out by adding 0.01 g MMT/HA/PVA@PPy into 10 mL Cr(VI) solution with a concentration of 50–250 mg/L, and isotherm adsorption tests were conducted at thermodynamic temperatures of 298, 308 and 318 K respectively. For the kinetic study, 0.01 g adsorbent was placed into 10 mL Cr(VI) solution with the concentration of 100 mg/L and pH 2 at 298 K, and the reaction was lasted for 10–600 min. In the continuous adsorption-desorption cycle experiment, 0.01 g MMT/HA/PVA@PPy was added into 10 mL Cr(VI) solution with the concentration of 100 mg/L and pH 2, and reacted at 298 K for 12 h. The adsorbent obtained by filtration was shaken for 2 h in 20 mL $Na_2CO_3$ solution with a concentration of 0.5 M to desorb Cr(VI). Then, the adsorbent was added into 20 mL HCl solution with a concentration of 2 M and shaken for 2 h to regenerate the adsorption active site. Cycle for four times to evaluate the regeneration ability of the adsorbent to remove Cr(VI) from water. Each group of experiments was conducted three times, and the average data were recorded and displayed. Langmuir and Freundlich isothermal models were used to study the adsorption capacity. Thermodynamic parameters were used to analyze the thermodynamic properties of the adsorption process. Pseudo-first-order model, pseudo-second-order model and intraparticle diffusion model were used to further study the adsorption and diffusion mechanism.

According to 1, 5-diphenylcarbazide spectrophotometry [48], the residual Cr(VI) ion concentration was measured using UV–Vis spectrophotometer (UV3600, Shimadzu Corporation), and converted into concentration value according to the standard curve. The removal rate R (%) of adsorbents for Cr(VI) and the equilibrium adsorbed Cr(VI) amount per gram of adsorbent $Q_e$ (mg/g) were calculated using Eqs. (1) and (2) as follows [49]:

$$R(\%) = \frac{C_0 - C_e}{C_0} \times 100 \tag{1}$$

$$Q_e = \frac{C_0 - C_e}{m} \times V \tag{2}$$

where $C_0$ (mg/L) and $C_e$ (mg/L) correspond to the initial and equilibrium concentrations of Cr(VI) ions, respectively. m(g) represents the mass of adsorbent, and V(L) represents the volume of Cr(VI) solution.

## 3 Results and Discussion

### 3.1 Characteristics of MMT/HA/PVA@PPy

The micro-morphology of Pickering emulsion droplets, MMT/HA/PVA and MMT/HA/PVA@PPy composites were characterized and analyzed. Figure 2a shows that the droplets of Pickering emulsion are evenly distributed, and the MMT/HA/PVA (Fig. 2b) and MMT/HA/PVA@PPy composite materials (Fig. 2c) prepared by using this Pickering emulsion as the template are all intact and have no collapse, and the pore size is equivalent to the droplet size of Pickering emulsion, which indicates that the template of Pickering emulsion prepared by using MMT/HA composite colloidal particles as the stabilizer has good stability. MMT/HA/PVA and MMT/HA/PVA@PPy have three-dimensional network structure, and there are abundant circular pores in the adsorbent with high connectivity. These pores can be used as water channels, so that the adsorbate can quickly reach the adsorption site with the water flow and combine with it, thus improving the adsorption rate of the material. Figure 2d shows that the MMT/HA/PVA has a smooth surface, while the surface of the composite MMT/HA/PVA@PPy (Fig. 2e) after PPy introduced becomes rough, and PPy is evenly distributed on the composite, which indicates that pyrrole is successfully compounded on the material, and the composite effectively avoids the agglomeration of PPy. The rough surface also provides more adsorption sites for Cr(VI) ions.

Figure 2f and g are EDX element analysis results of MMT/HA/PVA and composite adsorbent MMT/HA/PVA@PPy. The energy dispersion spectrum of MMT/HA/PVA is composed of C, N, O, Al, Si and Mg. However, after PPy was introduced, Cl element was added to the energy spectrum of the composite. Among them, Al, Si and Mg elements came from MMT, while Cl element came from

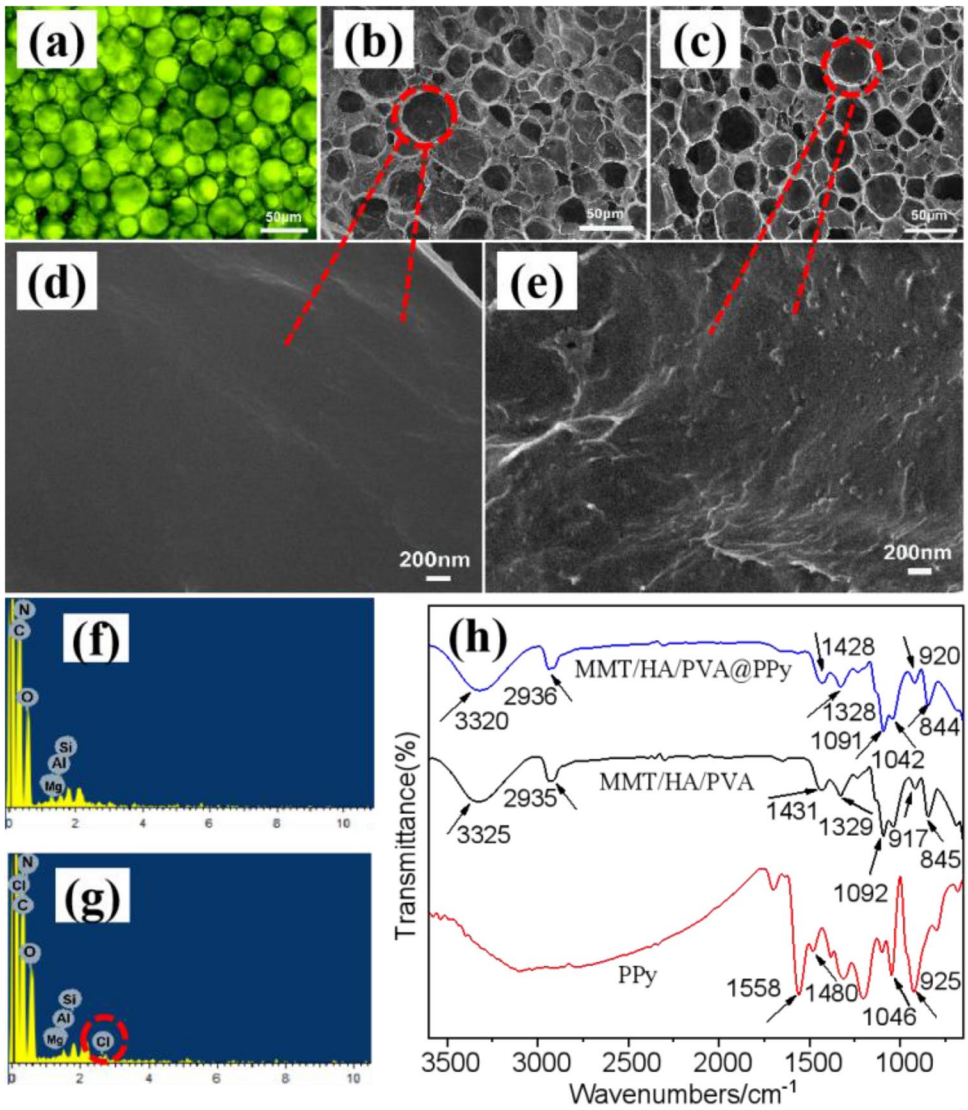


**Fig. 2** Optical microscope images of Pickering emulsion droplets (**a**), low magnification FESEM images of MMT/HA/PVA and MMT/HA/PVA@PPy (**b**, **c**), high magnification FESEM images of MMT/HA/PVA and MMT/HA/PVA@PPy (**d**, **e**), EDX analysis images of MMT/HA/PVA (**f**), MMT/HA/PVA@PPy (**g**) and FTIR spectra of PPy, MMT/HA/PVA, MMT/HA/PVA@PPy (**h**)

PPy-doped anion $Cl^-$. In addition, no peaks of other impurity elements were found, which indicated that all the materials were successfully compounded and the purity of the adsorbent was very high.

Figure 2h shows the infrared spectrum analysis results of PPy, MMT/HA/PVA and MMT/HA/PVA @PPy. There are four characteristic peaks in PPy curve, which correspond to C=C tensile vibration peak (1558 $cm^{-1}$), C–N tensile vibration peak (1480 $cm^{-1}$), C–H and N–H in-plane deformation vibration peak (1046 $cm^{-1}$), and C–H out-of-plane bending vibration peak (925 $cm^{-1}$), respectively [50, 51]. All of these peaks belong to the characteristic peak of PPy. In the MMT/HA/PVA curve, the tensile vibration peak of Si–O bond at 1092 $cm^{-1}$, the deformation vibration peak of –OH bond at 845 $cm^{-1}$ and the bending vibration peak of Al–OH bond at 917 $cm^{-1}$ indicate that MMT exists in the material [52]. C–C tensile vibration peak at 1431 $cm^{-1}$, CH– tensile vibration peak at 2935 $cm^{-1}$ and –OH tensile vibration peak at 3325 $cm^{-1}$ may come from PVA in the material [53]. In the spectrum of MMT/HA/ PVA@PPy, there are some characteristic peaks of PPy and MMT/HA/PVA, which indicate that PPy and MMT/HA/PVA have been successfully compounded.

X-ray diffraction (XRD) is often used to determine the degree of intercalation and/or exfoliation of clay. The Fig. 3 shows the X-ray diffraction patterns of the raw MMT and MMT/HA/PVA@PPy. It was observed that the raw MMT had a crystallization peak at 6.22°, but the XRD pattern of MMT/HA/PVA@PPy did not show any obvious peak, hence indicating that most of the MMT flakes in the adsorbent were exfoliated [54].

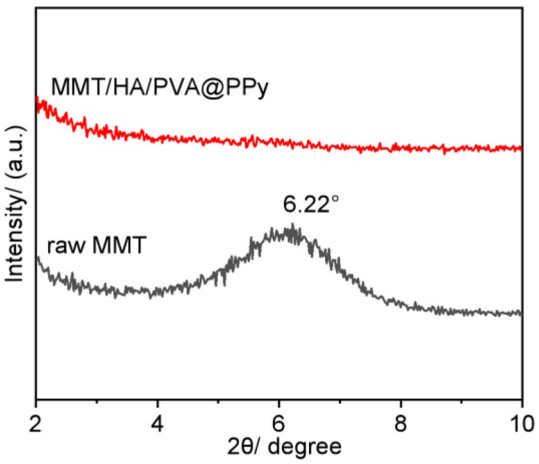


**Fig. 3** X-ray diffraction patterns of raw MMT and MMT/HA/PVA@PPy

**Table 1** Comparison on adsorption capacity of different samples

| Sample | Py content (%) | $q_e$ (mg/g) | Unit PPy adsorption capacity (mg/g) |
|---|---|---|---|
| MMT/HA/PVA | 0 | 44.02 ± 0.28 | 0 |
| PPy [55] | 100 | 21.87 | 21.87 |
| MMT/HA/PVA@PPy | 4.57 | 106.29 ± 0.45 | 1406.60 |

## 3.2 Adsorption Performance

### 3.2.1 Sorption Enhancement of Cr(VI) from Aqueous Solution by PPy Loaded on the Hydrogel

After subtracting the adsorption capacity of MMT/HA/PVA without conductive polymer, the adsorption capacity of PPy for Cr(VI) in MMT/HA/PVA@PPy composite was calculated according to the proportion of PPy, and it was compared with the adsorption capacity of pure PPy and MMT/HA/PVA in the literature. It can be seen from Table 1 that the adsorption of Cr(VI) by PPy in MMT/HA/PVA@PPy composites is much higher than that of pure PPy [55] and MMT/HA/PVA. Compared with the adsorption capacity of PPy in the literature (21.87 mg/g), the adsorption capacity of PPy in MMT/ HA/PVA@PPy for Cr(VI) (1406.60 mg/g-PPy) increased by about 64 times. This result is consistent with that expectation of experimental design. That is, the composite material can effectively avoid the problem that pyrrole is easy to agglomerate during polymerization, and significantly improve the adsorption capacity of the material. MMT/HA/PVA@PPy composite porous material has certain research value as Cr(VI) ion adsorbent.

### 3.2.2 Effect of pH

The pH value of solution is one of the key factors affecting the adsorption performance of materials. In this study, the effect of pH value of solution on the adsorption properties of MMT/HA/PVA@PPy composites was evaluated in the range of pH 2–10. The experimental results are shown in Fig. 4a. It can be seen that the adsorption capacity reaches its maximum at pH 2, and then the adsorption capacity decreases rapidly with the increase in pH value of the solution, because the surface charge of the adsorbent and the existing form of Cr(VI) ions in the aqueous solution are greatly affected by the pH value of the solution [56]. Figure 4b shows that Cr(VI) mainly exists in the form of $Cr_2O_7^{2-}$ or $HCrO_4^-$ anion in the pH range of 2–6 [57]. At this time, the surface of MMT/HA/PVA@PPy adsorbent is positively charged due to amino protonation, and Cr(VI) can be adsorbed by electrostatic attraction and chelation. On the other hand, $Cr_2O_7^{2-}$ and $HCrO_4^-$ ions can replace the doped $Cl^-$, and the adsorption reaction takes place through the ion exchange properties of PPy. In the aqueous solution with pH > 6, almost only $CrO_4^{2-}$ can exist stably [57], and the deprotonation of amino groups also reduces the positive charge on the surface of the adsorbent, which hinders the interaction with Cr(VI). In addition, the adsorbent will be de-doped, and excessive $OH^-$ may compete with $CrO_4^{2-}$ for

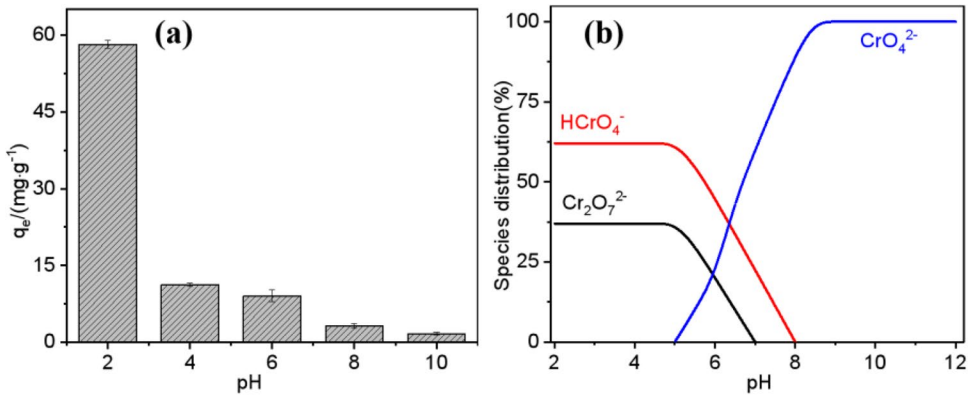


**Fig. 4** Effect of solution pH on adsorption performance (**a**) and species distribution of Cr(VI) at different pH (**b**)

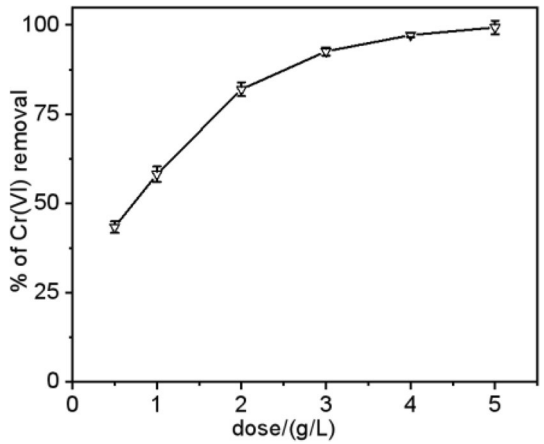


**Fig. 5** Effect of adsorbent dosage on adsorption performance

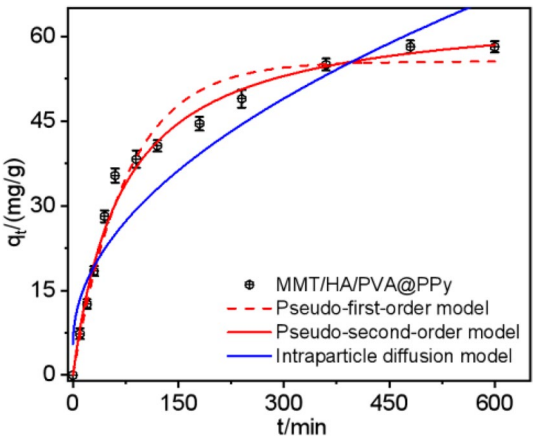


**Fig. 6** Kinetics of MMT/HA/PVA@PPy adsorption of Cr(VI)

adsorption sites, thus further reducing the adsorption capacity of the material.

### 3.2.3 Effect of Adsorbent Dose

Adsorbent dosage is one of the reference factors to weigh the cost and actual adsorption benefit. In this experiment, the effect of dosage on the adsorption of Cr(VI) by MMT/HA/PVA@PPy composites was studied in the range of 0.5–5 g/L. The results are shown in Fig. 5. Obviously, with the increase in dosage, the removal rate of Cr(VI) by MMT/HA/PVA@PPy also increased, and the removal rate increased slowly after reaching to 82%. With the further increase of dosage in 5 g/L, the removal rate of Cr(VI) reached 99.35%. In the process of increasing dosage from 0.5 to 1 g/L, a large number of adsorption active sites appeared, and the adsorption rate increased rapidly. With the continuous increase in dosage, the adsorption sites are saturated, the adsorption reaches equilibrium, and the adsorption rate increases slowly.

### 3.2.4 Adsorption Kinetics

Determining the adsorption equilibrium time of adsorbent is an important factor that must be considered when it is put into practical application. The effect of adsorption time on Cr(VI) adsorption of MMT/HA/PVA@PPy composites is shown in Fig. 6. In the initial 60 min, the adsorption rate increased rapidly with the increase of reaction time, because in the initial reaction stage, the adsorption reaction mainly occurs on the outer surface of the adsorbent, and there are a large number of available adsorption active sites on the adsorbent, the concentration of Cr(VI) in the local micro-environment of adsorbent-adsorbate is high. In the late stage of adsorption reaction, most of the adsorption active sites were occupied by Cr(VI), and the available active sites decreased. With the decrease of Cr(VI) concentration in the local micro-environment of adsorbent-adsorbate, the later adsorption rate gradually slows down until the adsorption equilibrium is reached.

The adsorption kinetics was studied to understand the adsorption process of Cr(VI) on MMT/HA/PVA@PPy adsorbent. The results are shown in Fig. 6. Pseudo-first-order model, pseudo-second- order model and intraparticle diffusion model [58] are used to fit the kinetic data to preliminarily understand the kinetic mechanism of the adsorbent. The nonlinear equations are expressed as follows:

$$\text{Pseudo-first-order: } q_t = q_e\left(1 - e^{-k_1 t}\right) \tag{3}$$

$$\text{Pseudo-second-order: } q_t = \frac{k_2 q_e^2 t}{1 + k_2 q_e t} \tag{4}$$

$$\text{Intraparticle diffusion model: } q_t = k_3 t^{0.5} + C \tag{5}$$

where $k_1$ (1/min) and $k_2$ (g/(mg min)) are Pseudo-first-order and Pseudo-second order rate constants, respectively. $q_t$ (mg/g) is the amount of Cr(VI) adsorbed at time t, $q_e$ (mg/g) is equilibrium adsorption amount, $k_3$ (mg/(g $min^{0.5}$)) is the Intraparticle diffusion constant, and C is the boundary layer thickness constant.

From Fig. 6 and Table 2, it can be seen that the correlation coefficient ($R^2 = 0.912$) obtained by fitting the adsorption data with the intraparticle diffusion model is poor, the constant C value is not 0, and the fitting curve does not pass through the origin of coordinates, which shows that the intraparticle diffusion is not the only rate control factor in the adsorption process of Cr(VI) [59]. The fitting results of kinetic model show that the correlation coefficient of pseudo-second-order adsorption rate equation ($R^2 = 0.992$) is higher than that of pseudo-first-order adsorption rate equation ($R^2 = 0.981$), and the adsorption process of MMT/

**Table 2** Adsorption kinetic models and parameters for removal of Cr(VI) on MMT/HA/PVA@PPy

| Models | Parameters | |
|---|---|---|
| | $C_0$ (mg/L) | 100 |
| | $q_e$(exp) (mg/g) | 58.16 |
| Pseudo-first-order | $k_1$ (1/min) | 0.014 |
| | $q_e$ (mg/g) | 50.05 |
| | $R^2$ | 0.981 |
| Pseudo-second-order | $k_2$ (g/(mg min)) | 0.0002 |
| | $q_e$ (mg/g) | 63.50 |
| | $R^2$ | 0.992 |
| Intraparticle diffusion | $k_3$ (mg/(g $min^{0.5}$)) | 2.511 |
| | C | 5.516 |
| | $R^2$ | 0.912 |

HA/PVA@PPy composites follows the pseudo-second-order kinetic model. Moreover, the calculated value $q_e$ (63.50 mg/g) of the pseudo-second-order kinetic model is closer to the experimental value $q_e$ (58.16 mg/g), which further confirms this point. The pseudo-second-order kinetic model holds that the adsorption of Cr(VI) on MMT/HA/PVA@PPy composites is a process dominated by chemical adsorption. The above results indicated the main rate-limiting step should be a chemical adsorption involving valence forces through exchanging of electrons between adsorbent and adsorbate [60, 61].

### 3.2.5 Adsorption Isotherm

Two isotherm models, namely Langmuir model [62] (monolayer homogeneous adsorption) and Freundlich model [63] (multilayer heterogeneous adsorption) are used to fit the experimental data, so as to further study the interaction between adsorbate and adsorbent and the adsorption capacity of adsorbent. The equations of the two models are as follows:

$$\text{Langmuir: } q_e = \frac{K_L q_m C_e}{1 + K_L C_e} \tag{6}$$

$$\text{Freundlich: } q_e = K_F C_e^{1/n} \tag{7}$$

where $C_e$ is the Cr (VI) mass concentration in solution equilibrium (mg/L), $q_e$ is equilibrium adsorption amount (mg/g), $q_m$ is the maximum adsorption capacity (mg/g), $K_L$ is the Langmuir constant related to adsorption energy (L/mg), $K_F$ and n are Freundlich isotherm parameters related to adsorption capacity (mg/g) and adsorption strength respectively.

The fitting results of isotherm models are shown in Fig. 7a and Table 3. With the increase of the initial concentration of Cr(VI) in the solution, the adsorption capacity of MMT/HA/PVA@PPy also increases. In addition, the adsorption capacity increases with the increase of temperature, reaching the optimal adsorption capacity of 106.29 mg/g at 318 K. This indicates that the adsorption process may have experienced chemical interaction rather than physical interaction. The increase in adsorption capacity is due to the increase in collision frequency between adsorbent and adsorbate, which leads to the enhanced adsorption of Cr(VI) ions in aqueous solution. The initial concentration and reaction temperature have positive correlation to the adsorption performance of the material, and the adsorption process of the material is

**Table 3** Adsorption isotherm models and parameters for removal of Cr(VI) on MMT/HA/PVA@PPy

| Model | Parameter | Temperature (K) | | |
|---|---|---|---|---|
| | | 298 | 308 | 318 |
| Langmuir | $q_m$ (mg/g) | 102.64 | 103.78 | 106.39 |
| | $K_L$ (L/mg) | 0.041 | 0.099 | 0.206 |
| | $R^2$ | 0.972 | 0.979 | 0.985 |
| Freundlich | $K_F$ (mg/g) | 17.57 | 27.37 | 39.02 |
| | 1/n | 0.327 | 0.269 | 0.208 |
| | $R^2$ | 0.963 | 0.977 | 0.967 |

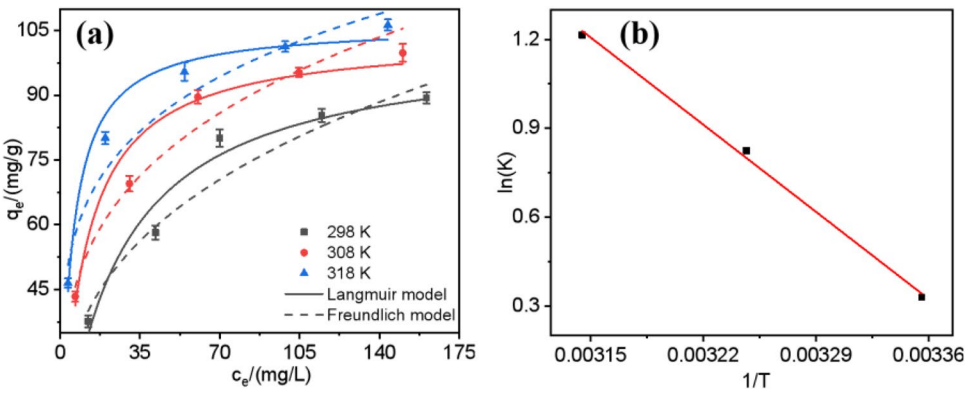


**Fig. 7** Isotherms of MMT/HA/PVA@PPy adsorption of Cr(VI) with fittings of Langmuir and Freundlich models (**a**), and plot of ln(K)–1/T to determine the thermodynamic parameters of Cr(VI) adsorption onto MMT/HA/PVA@ PPy (**b**)

**Table 4** Comparison on Cr(VI) adsorption of MMT/HA/PVA@PPy with other PPy-based adsorbents

| Adsorbent | $q_m$ (mg/g) | pH | Initial Cr(VI) concentration (mg/L) | References |
|---|---|---|---|---|
| PPy/$Fe_3O_4$/ATP composite | 43.48 | 2.0 | 100–500 | [64] |
| PPy/Mg–Al layer double hydroxides (LDHs) | 76.21 | 5.0 | 10–50 | [65] |
| Calcium-aluminum-layered double hydroxide/PPy | 66.14 | 2.0 | 30–400 | [66] |
| PPy@magnetic chitosan | 105 | 4.5 | 20–200 | [67] |
| MMT/HA/PVA@PPy | 106.29 | 2.0 | 50–250 | This study |

an endothermic reaction process. Compared with Freundlich model, Langmuir model is more consistent with isotherm data, and more suitable for describing the adsorption process of Cr(VI) by MMT/HA/PVA@PPy, suggesting that the adsorption of Cr(VI) on the composite is in the form of a single layer, and the active sites are evenly distributed on the material. Comparing the adsorption of Cr(VI) by MMT/HA/PVA@PPy with other PPy-based materials (Table 4), it is found that MMT/HA/PVA@PPy has a high adsorption capacity for removing Cr(VI), and the best adsorption capacity can reach 106.29 mg/g at 318 K, which is higher than that of most literature materials. It is expounded that MMT/HA/PVA@PPy has a wide application prospect in removing Cr(VI).

### 3.2.6 Thermodynamics Studies

In order to study the thermodynamic properties of adsorption process, the following thermodynamic parameters were calculated. Thermodynamic parameters such as standard Gibbs free energy change ($\Delta G^0$), enthalpy change ($\Delta H^0$) and entropy change ($\Delta S^0$) for the adsorption of Cr(VI) by MMT/HA/PVA@PPy (initial concentration of 100 mg/L) have been determined by the following equations [68]:

$$\Delta G^0 = -RT \ln K \tag{8}$$

$$\ln K = \frac{\Delta S^0}{R} - \frac{\Delta H^0}{RT} \tag{9}$$

$$K = \frac{q_e}{C_e} \tag{10}$$

where R is the ideal gas constant 8.314 J/mol K, T is temperature (K), m is adsorbent dosage (g/L), and K is thermodynamic equilibrium constant (L/g). The values of $\Delta H^0$ and $\Delta S^0$ come from the slope and intercept of ln(K)–1/T diagram (Fig. 7b). The thermodynamic parameters obtained are shown in Table 5. The positive value of $\Delta H^0$ confirms that the adsorption reaction is an endothermic process, and the high temperature promotes the removal of Cr(VI), which is consistent with the results discussed by isotherm models. The positive value of $\Delta S^0$ indicates that the disorder of the solid–liquid interface increases during the adsorption process, indicating that the adsorbate and adsorbent have changed during the adsorption process. At all experimental temperatures, $\Delta G^0$ is negative, which indicates that the adsorption process of Cr(VI) is spontaneous and feasible [69]. The values of $\Delta G^0$ are − 3.44, − 5.84 and − 8.92 kJ/mol, respectively, which decrease with the increase of temperature, indicating that the increase of temperature is beneficial to adsorption.

**Table 5** Thermodynamic parameters for removal of Cr(VI) on MMT/HA/PVA@PPy

| T(K) | Thermodynamic parameter | | |
|---|---|---|---|
| | $\Delta G^0$ (kJ/mol) | $\Delta H^0$ (kJ/mol) | $\Delta S^0$ (kJ/mol/K) |
| 298 | − 3.44 | 34.947 | 0.120 |
| 308 | − 5.84 | | |
| 318 | − 8.92 | | |

### 3.2.7 Desorption and Regeneration Studies

The regenerability of adsorbent is an important index to evaluate the practical application potential of the prepared adsorbent. In this experiment, $NaHCO_3$ (0.5 M) solution was used to treat the adsorbent after adsorbing Cr(VI), which could promote the deprotonation of surface functional groups and desorb Cr(VI) on the adsorbent. Then HCl (2M) solution was used as dopant to reactivate the adsorption site. Four adsorption–desorption cycles were used to evaluate the regeneration ability of adsorbent to remove Cr(VI). The Fig. 8 shows the removal efficiency of MMT/HA/PVA@PPy in each adsorption cycle. After four cycles, the removal capacity of Cr(VI) by MMT/HA/PVA@PPy decreased from 58.16 to 30.11 mg/g. The decrease of removal efficiency might be owing to the fact that Cr(VI) is not completely desorbed from the adsorbent or that the undesorbed Cr(III) occupies part of the active sites [70]. The results showed that MMT/HA/PVA@PPy composite porous hydrogel has good regenerability, and it is an effective adsorbent for treating Cr(VI) ion polluted wastewater.

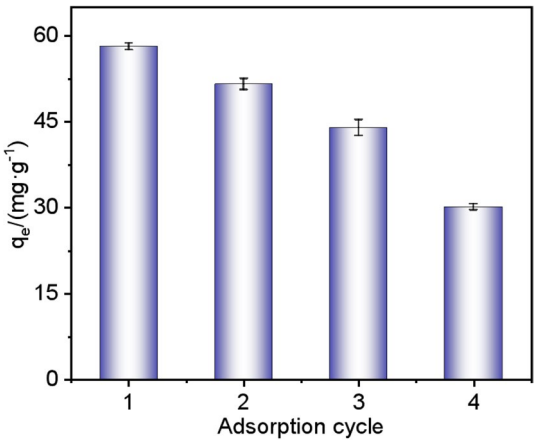


**Fig. 8** Regeneration cycle of MMT/HA/PVA@PPy adsorption of Cr(VI)

### 3.2.8 Adsorption Mechanism

As shown in Fig. 9a and b, and compared with Fig. 2c and e, it is found that there is no obvious change in the structure of the material before and after adsorption, which indicates that the structure of the prepared composite material is stable, and the structure of the material is not damaged by adsorption and recovery treatment. Figure 9c shows the EDX element spectrum of the material after adsorption. Compared with that before adsorption (Fig. 2g), it is found that the obvious Cr element peak appears in the energy spectrum after adsorption, but the Cl element peak disappears, which indicates that a large number of Cr(VI) ions are adsorbed on MMT/HA/PVA@PPy composites by substituting the doped $Cl^-$. EDX analysis has clearly revealed the presence of Cr element on the MMT/HA/PVA@PPy composite.

The results of isotherm and kinetic analysis show that chemisorption plays an important role in the whole adsorption process, and other mechanisms may also contribute to

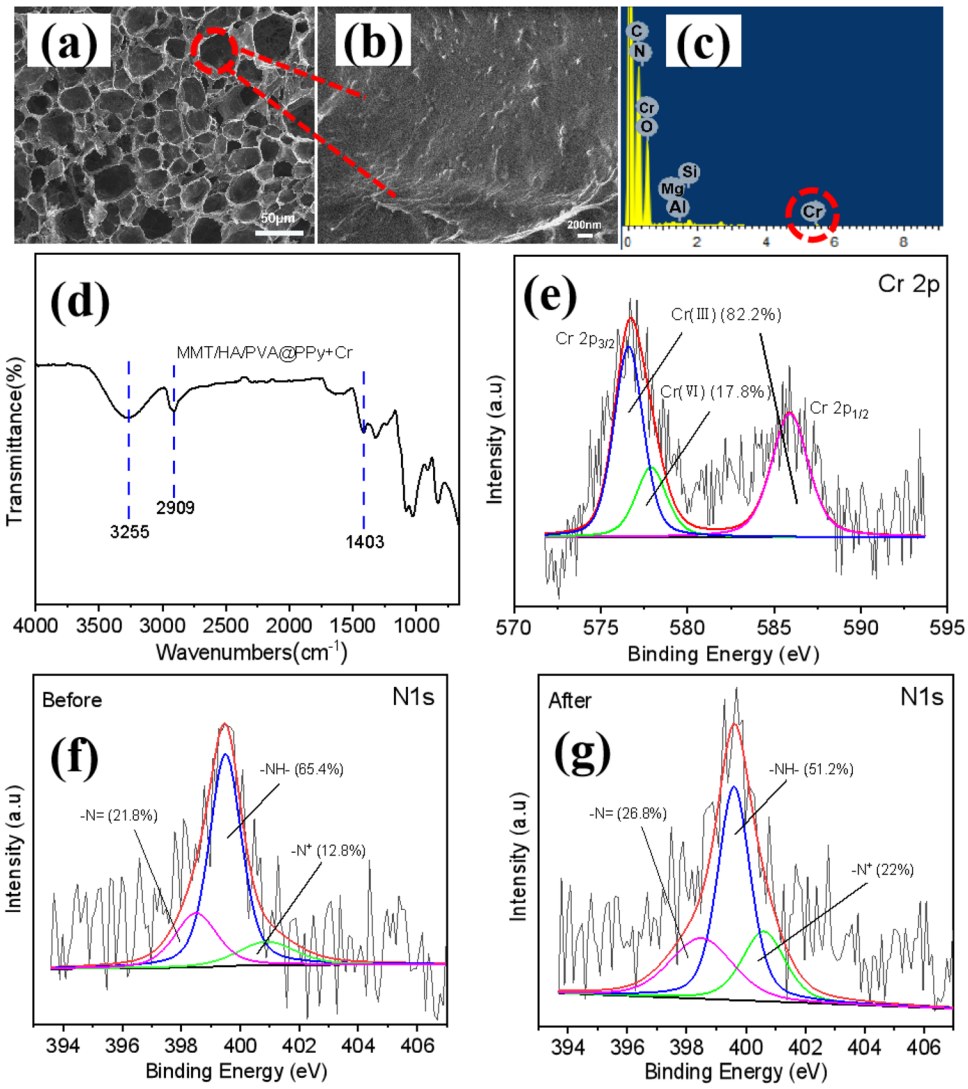


**Fig. 9** Low and high magnification FESEM (**a**, **b**), EDX (**c**), FTIR plots (**d**) and high-resolution XPS spectra of Cr 2p (**e**) of MMT/HA/PVA@PPy after Cr(VI) adsorption, high-resolution XPS spectra of N 1s (**f**, **g**) of MMT/HA/PVA @PPy before and after Cr(VI) adsorption

adsorption. Therefore, by comparing the FTIR spectra of MMT/HA/PVA@PPy composites before and after adsorption, we analyzed the possible mechanism of Cr(VI) adsorption. Comparing the spectrum of MMT/HA/PVA@ PPy in Fig. 9d with that in Fig. 2h, it is found that after Cr(VI) adsorption, all peaks move to a low wave number, which is caused by the delocalized π electrons in PPy matrix which participate in the vibration of PPy ring skeleton are affected by doping ions in polymer matrix. It is speculated that Cr(VI) anion replaces the doped anion $Cl^-$, which may interfere with the conjugated structure of PPy, limit the delocalization degree of the charge along the polymer chain, and lead to the red shift of the peak [71]. The in-plane deformation vibration peak of N–H at 1403 $cm^{-1}$ is obviously weakened after adsorption, indicating that amino functional groups are the main participating groups in the adsorption reaction. Meanwhile, the peaks of CH– tensile vibration and –OH tensile vibration at 3255 $cm^{-1}$ and 2909 $cm^{-1}$ are also weakened after adsorption, and it was judged that the hydrogel structure as a carrier may also have some adsorption effect on Cr(VI). As far as the overall spectrum is concerned, the peaks before and after adsorption of Cr(VI) remain basically unchanged, but some peaks have a slight change in displacement and intensity, which shows that the adsorbed Cr(VI) does not destroy the structure of the adsorbent itself [72]. It is consistent with the results of FESEM analysis after adsorption.

In order to further analyze the adsorption mechanism of MMT/HA/PVA@PPy for Cr(VI), the high-resolution XPS spectrum of the adsorbent before and after Cr(VI) adsorption was analyzed. Figure 9e reveals the high-resolution XPS spectra of Cr 2p of MMT/HA/PVA@PPy after Cr(VI) adsorption. After the adsorption, the spectra of Cr 2p were fitted into three peaks at 576.6 (Cr $2p_{3/2}$), 585.9 (Cr $2p_{1/2}$) and 577.9 (Cr $2p_{3/2}$) eV, the former two were assigned to Cr(III) and the last one was Cr(VI) [21]. The presence of Cr(VI) was mainly attributed to the anion exchange by replacing the $Cl^-$ which was from acid etching, and the electrostatic interaction with protonated amino groups. Approximately 82.2% of the attached Cr(VI) can be reduced to Cr(III), while 17.8% can be directly absorbed by the adsorbent in the form of Cr(VI). The existence of Cr(III) proves the occurrence of redox reaction. The above results confirm that Cr(VI) was adsorbed onto the materials, and more importantly, the in-situ chemical reduction of Cr(VI) to Cr(III) occurred during the adsorption process.

As we all know, the reduction of Cr(VI) to Cr(III) requires the participation of electron donors. According to reports, amino groups, carboxyl groups and hydroxyl groups can all react with Cr(VI) as electron donors [66]. So, the N categories of PPy fierce play cruel roles in the reduction of Cr (VI) process. Figure 9f and g reveals the N 1s high-resolution XPS spectra of MMT/HA/PVA@PPy of before and after Cr(VI) adsorption. As shown in Fig. 9f, the N 1s XPS spectra of original MMT/HA/PVA@PPy composite can be deconvoluted into three different peaks at 398.5, 399.5 and 400.9 eV, which were attributed into 21.8% of imine nitrogen (–N=), 65.4% of amine nitrogen (–NH–), and 12.8% of charged nitrogen ($–N^+$) groups respectively. It should be noted that the formation of ($–N^+$) is due to the protonation of some imines caused by the addition of hydrochloric acid during the synthesis process [73]. After Cr(VI) adsorption, the N 1 s XPS spectrum of MMT/HA/PVA@PPy composites can still be deconvolved into three different peaks (Fig. 9g), but the percentage of nitrogen component have changed. Among them, the percentage of –N=, –NH– and $–N^+$ groups changed to 26.8, 51.2, and 22%, respectively. Obviously, the percentage of –NH– decreased, while the percentage of –N= increased significantly, further confirmed the occurrence of redox reaction along with the adsorption process and –NH– groups acted as electron donors [74]. Meanwhile, the increase in the percentage of $–N^+$ is consistent with the decrease in pH in the solution after adsorption.

Overall, the results of XPS spectrum analysis show that Cr(VI) can be adsorbed on MMT/HA/ PVA@PPy composites through ion exchange and electrostatic interaction, and part of Cr(VI) can be converted into less toxic Cr(III) through redox reaction, in which nitrogen-containing groups are the main participating groups, especially in the reduction process.

## 4 Conclusions

In this experiment, MMT/HA/PVA Pickering emulsion was prepared by using MMT/HA colloidal particles obtained by modifying MMT with humic acid (HA) as stabilizer. Under acidic conditions, the positively charged Pyrrole monomer was deposited on the emulsion droplet interface due to electrostatic interaction with negatively charged MMT/HA, and MMT/HA/PVA@PPy composite was prepared by Pickering emulsion template-in-situ chemical oxidation polymerization. Surprisingly, the maximum adsorption of Cr(VI) by PPy in MMT/HA/PVA@PPy can reach 1406.49 mg/g-PPy, which is almost 64-times that of pure PPy (21.87 mg/g). The adsorption of Cr(VI) by MMT/HA/PVA@PPy is more in line with the pseudo-second-order kinetic model, mainly chemical adsorption. The intraparticle diffusion model shows that the adsorption process is carried out jointly by intraparticle diffusion and membrane diffusion. The adsorption behavior is more suitable to be fitted by Langmuir model, which belongs to single-layer homogeneous adsorption. Thermodynamic parameters prove that Cr(VI) adsorption is a spontaneous endothermic reaction. The mechanisms of removing Cr(VI) by MMT/HA/PVA@PPy may be mainly ion exchange, electrostatic interaction

and redox. The composite material has a great application prospect, and this work provides a new idea and technology for the efficient utilization of conductive polymers and the successful treatment of heavy metal ions in wastewater.

**Author Contributions** All authors contributed to the study conception and design. XZ: process the data and write the manuscript. YL, WZ, LD: work together to complete material preparation, data collection and analysis. JC: directed, revised, and supplemented the manuscript. All authors commented on previous versions of the manuscript, and all authors read and approved the final manuscript.

**Funding** This work was supported by Preparation of lignite humic acid-based magnetic composite microspheres and their adsorption properties for heavy metal ions, National Natural Science Foundation of China (21576001), and the National College Students Innovation and Entrepreneurship Training Program (202110360041).

**Data Availability Statement** Not applicable.

## Declarations

**Conflict of Interest** The authors confirm that there is no conflict of interest for this paper.

## References

1. A.M. Hezma, W.A. Shaltout, H.A. Kabary, G.S. El-Bahy, A.B. Abdelrazzak, Fabrication, characterization and adsorption investigation of nano zinc oxide-sodium alginate beads for effective removal of chromium (VI) from aqueous solution. J. Inorg. Organomet. Polym. Mater. (2023). https://doi.org/10.1007/s10904-023-02573-4
2. V.P. Dinh, M.D. Nguyen, Q.H. Nguyen, T.T. Do, T.T. Luu, A.T. Luu, T.D. Tap, T.H. Ho, T.P. Phan, T.D. Nguyen, L.V. Tan, Chitosan-$MnO_2$ nanocomposite for effective removal of Cr (VI) from aqueous solution. Chemosphere **257**, 127147 (2020). https://doi.org/10.1016/j.chemosphere.2020.127147
3. X.X. Zhang, G.Y. Yi, Z.T. Zhang, J. Yu, H.Y. Fan, P. Li, H.H. Zeng, B.L. Xing, L. Chen, C.X. Zhang, Magnetic graphene-based nanocomposites as highly efficient absorbents for Cr(VI) removal from wastewater. Environ. Sci. Pollut. Res. **28**(12), 14671–14680 (2021). https://doi.org/10.1007/s11356-020-11634-x
4. X.Z. Sun, P. Guo, Y.Y. Sun, Y.Q. Cui, Adsorption of hexavalent chromium by sodium alginate fiber biochar loaded with lanthanum. Materials (2021). https://doi.org/10.3390/ma14092224
5. Y. Tadjenant, N. Dokhan, A. Barras, A. Addad, R. Jijie, S. Szunerits, R. Boukherroub, Graphene oxide chemically reduced and functionalized with KOH-PEI for efficient Cr(VI) adsorption and reduction in acidic medium. Chemosphere **258**, 127316 (2020). https://doi.org/10.1016/j.chemosphere.2020.127316
6. G. Angeline Divya, R. Sakthibalan, K. Sumithra Parvadha Varthini, K. Deepa, S. Samdavid, Experimental investigation of hydrodynamics and chromium(VI) adsorption in continuous countercurrent fluidized column. Chem. Pap. **74**(4), 1281–1288 (2019). https://doi.org/10.1007/s11696-019-00977-6
7. Y.L. Bin, Q.W. Liang, H.J. Luo, Y.Y. Chen, T. Wang, One-step synthesis of nitrogen-functionalized graphene aerogel for efficient removal of hexavalent chromium in water. Environ. Sci. Pollut. Res. **30**, 6746–6757 (2022). https://doi.org/10.1007/s11356-022-22591-y
8. R. Sinha, R. Kumar, P. Sharma, N. Kant, J. Shang, T.M. Aminabhavi, Removal of hexavalent chromium via biochar-based adsorbents: state-of-the-art, challenges, and future perspectives. J. Environ. Manag. **317**, 115356 (2022). https://doi.org/10.1016/j.jenvman.2022.115356
9. E. Parthiban, N. Kalaivasan, S. Sudarsan, Dual responsive (pH and magnetic) nanocomposites based on $Fe_3O_4$@polyaniline/itaconic acid: synthesis, characterization and removal of toxic hexavalent chromium from tannery wastewater. J. Inorg. Organomet. Polym. Mater. **30**(11), 4677–4690 (2020). https://doi.org/10.1007/s10904-020-01602-w
10. H. Karimi-Maleh, A. Ayati, S. Ghanbari, Y. Orooji, B. Tanhaei, F. Karimi, M. Alizadeh, J. Rouhi, L. Fu, M. Sillanpää, Recent advances in removal techniques of Cr(VI) toxic ion from aqueous solution: a comprehensive review. J. Mol. Liq. **329**, 115062 (2021). https://doi.org/10.1016/j.molliq.2020.115062
11. S.W. Lv, J.M. Liu, Z.H. Wang, H. Ma, C.Y. Li, N. Zhao, S. Wang, Recent advances on porous organic frameworks for the adsorptive removal of hazardous materials. J. Environ. Sci. **80**, 169–185 (2019). https://doi.org/10.1016/j.jes.2018.12.010
12. A. Taghizadeh, M. Taghizadeh, M. Jouyandeh, M.K. Yazdi, P. Zarrintaj, M.R. Saeb, E.C. Lima, V.K. Gupta, Conductive polymers in water treatment: a review. J. Mol. Liq. **312**, 113447 (2020). https://doi.org/10.1016/j.molliq.2020.113447
13. S. Maity, A. Dubey, S. Chakraborty, A review on polypyrrole-coated bio-composites for the removal of heavy metal traces from waste water. J. Ind. Text. **51**(1), 152–173 (2019). https://doi.org/10.1177/1528083719871272
14 A.A. Alghamdi, A.B. Al-Odayni, W.S. Saeed, A. Al-Kahtani, F.A. Alharthi, T. Aouak, Efficient adsorption of lead (II) from aqueous phase solutions using polypyrrole-based activated carbon. Materials (2019). https://doi.org/10.3390/ma12122020
15. W. Mao, Y. Zhang, J.E. Luo, L.T. Chen, Y.T. Guan, Novel copolymerization of polypyrrole/polyaniline on ferrate modified biochar composites for the efficient adsorption of hexavalent chromium in water. Chemosphere **303**(Pt 3), 135254 (2022). https://doi.org/10.1016/j.chemosphere.2022.135254
16. Y.T. Shao, Z.H. Fan, M.F. Zhong, W. Xu, C. He, Z.J. Zhang, Polypyrrole/bacterial cellulose nanofiber composites for hexavalent chromium removal. Cellulose **28**(4), 2229–2240 (2021). https://doi.org/10.1007/s10570-020-03660-2
17. J. Chen, X.Q. Hong, Q.D. Xie, D.K. Li, Q.F. Zhang, Sepiolite fiber oriented-polypyrrole nanofibers for efficient chromium(VI) removal from aqueous solution. J. Chem. Eng. Data **59**(7), 2275–2282 (2014). https://doi.org/10.1021/je500319a
18. L. Mdlalose, M. Balogun, K. Setshedi, L. Chimuka, A. Chetty, Performance evaluation of polypyrrole–montmorillonite clay composite as a re-usable adsorbent for Cr(VI) remediation. Polym. Bull. **78**(8), 4685–4697 (2020). https://doi.org/10.1007/s00289-020-03338-6
19. V.D. Thao, B.L. Giang, T.V. Thu, Free-standing polypyrrole/polyaniline composite film fabricated by interfacial polymerization at the vapor/liquid interface for enhanced hexavalent chromium adsorption. RSC. Adv. **9**(10), 5445–5452 (2019). https://doi.org/10.1039/c8ra10478f
20 X. Ye, Q.C. Xu, J. Xu, Oxidant-templating fabrication of pure polypyrrole hydrogel beads as a highly efficient dye adsorbent. RSC Adv. **9**(11), 5895–5900 (2019). https://doi.org/10.1039/c9ra00209j
21. Y.Q. Zhan, S.J. He, X.Y. Wan, J.M. Zhang, B.C. Liu, J.F. Wang, Z.Y. Li, Easy-handling bamboo-like polypyrrole nanofibrous mats with high adsorption capacity for hexavalent chromium removal. J. Colloid Interface Sci. **529**, 385–395 (2018). https://doi.org/10.1016/j.jcis.2018.06.033
22. S. Gao, Z.C. Liu, Q.S. Yan, P. Wei, Y. Li, J.Y. Ji, L. Li, Facile synthesis of polypyrrole/reduced graphene oxide composite

hydrogel for Cr(VI) removal. J. Inorg. Organomet. Polym. Mater. **31**(9), 3677–3685 (2021). https://doi.org/10.1007/s10904-021-02037-7
23. M. Hasanpour, M. Hatami, Application of three dimensional porous aerogels as adsorbent for removal of heavy metal ions from water/wastewater: a review study. Adv. Colloid Interface Sci. **284**, 102247 (2020). https://doi.org/10.1016/j.cis.2020.102247
24. G.J. Zhang, H.Y. Chen, G.J. Yang, H. Fu, Preparation of in situ ZIF-9 grown on sodium alginate/polyvinyl alcohol hydrogels for enhancing Cu(II) adsorption from aqueous solutions. J. Inorg. Organomet. Polym. Mater. **32**(12), 4576–4588 (2022). https://doi.org/10.1007/s10904-022-02463-1
25. B. Taşdelen, D.İ Çifçi, S. Meriç, Preparation and characterization of chitosan/AMPS/kaolinite composite hydrogels for adsorption of methylene blue. Polym. Bull. **79**(11), 9643–9662 (2021). https://doi.org/10.1007/s00289-021-03970-w
26. B. Yan, J. Lan, Y.S. Li, Y.J. Peng, L.Y. Shi, R. Ran, Hexagonal $Ni(OH)_2$ nanosheets for stabilizing Pickering emulsion and Congo red adsorption. Colloids Surf. A: Physicochem. Eng. Asp. **598**, 124828 (2020). https://doi.org/10.1016/j.colsurfa.2020.124828
27. S.U. Pickering, CXCVI.—Emulsions. J. Chem. Soc. Trans. **91**, 2001–2021 (1907). https://doi.org/10.1039/ct9079102001
28. Z. Li, X.X. Jiang, Z.H. Yao, F.C. Chen, L. Zhu, H.N. Liu, L.S. Ming, Chitosan functionalized cellulose nanocrystals for stabilizing Pickering emulsion: fabrication, characterization and stability evaluation. Colloids Surf. A: Physicochem. Eng. Asp. **632**, 127769 (2022). https://doi.org/10.1016/j.colsurfa.2021.127769
29. Z. Khalaj-Amirhosseini, M. Ashjari, R. Jamjah, H. Arabi, M. Nazarabi, Emulsion based nanoarchitectonics for styrene–butyl acrylate copolymerization upon Pickering mechanism. J. Inorg. Organomet. Polym. Mater. **32**(3), 864–874 (2022). https://doi.org/10.1007/s10904-022-02224-0
30. Y.F. Zhu, W.B. Wang, H. Yu, A.Q. Wang, Preparation of porous adsorbent via Pickering emulsion template for water treatment: a review. J. Environ. Sci. **88**, 217–236 (2020). https://doi.org/10.1016/j.jes.2019.09.001
31. J.G. Yu, Y. Jin, G.Q. Liu, F.Q. Hua, Y.W. Lv, Pickering emulsion templated strategy in composite aerogels with hierarchical porous structure improves thermal insulation and diphenylamine adsorption. J. Appl. Polym. Sci. **139**(19), 52130–52141 (2022). https://doi.org/10.1002/app.52130
32. N. Higashide, N. Matsuda, K. Naoe, M. Imai, Application of food-grade magnesium stearate microparticles as stabilizer in preparation of biocompatible Pickering emulsions. Chem. Pap. **75**(4), 1639–1648 (2020). https://doi.org/10.1007/s11696-020-01428-3
33. Z. Sun, X.X. Yan, Y. Xiao, L.J. Hu, M. Eggersdorfer, D. Chen, Z.Z. Yang, D.A. Weitz, Pickering emulsions stabilized by colloidal surfactants: role of solid particles. Particuology **64**, 153–163 (2022). https://doi.org/10.1016/j.partic.2021.06.004
34 Z. Wang, Y.P. Wang, Tuning amphiphilicity of particles for controllable Pickering emulsion. Materials (2016). https://doi.org/10.3390/ma9110903
35. T.T. Lu, H. Gou, H.H. Rao, G.H. Zhao, Recent progress in nanoclay-based Pickering emulsion and applications. J. Environ. Chem. Eng. **9**(5), 105941 (2021). https://doi.org/10.1016/j.jece.2021.105941
36. J.H. Shin, J.W. Park, H.J. Kim, Clay-polystyrene nanocomposite from Pickering emulsion polymerization stabilized by vinylsilane-functionalized montmorillonite platelets. Appl. Clay Sci. **182**, 105288 (2019). https://doi.org/10.1016/j.clay.2019.105288
37 A. Olad, M. Bastanian, H. Bakht Khosh Hagh, Thermodynamic and kinetic studies of removal process of hexavalent chromium ions from water by using bio-conducting starch-montmorillonite/polyaniline nanocomposite. J. Inorg. Organomet. Polym. Mater. **29**(6), 1916–1926 (2019). https://doi.org/10.1007/s10904-019-01152-w
38. Y. Chu, S. Zhu, M. Xia, F. Wang, W. Lei, Methionine-montmorillonite composite—a novel material for efficient adsorption of lead ions. Adv. Powder Technol. **31**(2), 708–717 (2020). https://doi.org/10.1016/j.apt.2019.11.026
39. H. Zhang, J. Ma, F. Wang, Y. Chu, L. Yang, M. Xia, Mechanism of carboxymethyl chitosan hybrid montmorillonite and adsorption of Pb(II) and Congo red by CMC-MMT organic-inorganic hybrid composite. Int. J. Biol. Macromol. **149**, 1161–1169 (2020). https://doi.org/10.1016/j.ijbiomac.2020.01.201
40. B. Yao, Y. Liu, D. Zou, Removal of chloramphenicol in aqueous solutions by modified humic acid loaded with nanoscale zero-valent iron particles. Chemosphere **226**, 298–306 (2019). https://doi.org/10.1016/j.chemosphere.2019.03.098
41 Y. Chen, W. Jiang, C. Zhao, Z. Liu, Y. Liang, Facile modification of graphene oxide by humic acid for enhancing hexavalent chromium photoreduction. J. Environ. Chem. Eng. (2021). https://doi.org/10.1016/j.jece.2020.104759
42 H. Lu, J. Wang, F. Li, X. Huang, B. Tian, H. Hao, Highly efficient and reusable montmorillonite/Fe(3)O(4)/humic acid nanocomposites for simultaneous removal of Cr(VI) and aniline. Nanomaterials (2018). https://doi.org/10.3390/nano8070537
43. K. Jiang, A. Xiang, K. Liu, Q. Peng, Potential of montmorillonite and humus-like substances modified montmorillonite for remediation of Pb and Zn-contaminated soils. Appl. Clay Sci. (2023). https://doi.org/10.1016/j.clay.2023.106853
44. W.S. Jemima, P. Magesan, P. Chiranjeevi, M.J. Umapathy, Sorption properties of organo modified montmorillonite clay for the reclamation of chromium (VI) from waste water. Silicon **11**(2), 925–933 (2018). https://doi.org/10.1007/s12633-018-9887-z
45. S. Majumdar, R. Moral, D. Mahanta, Rapid mixing polymerization: a simple method for preparation of free standing polypyrrole film and powder for the removal of anionic pollutants. Colloids Surf. A: Physicochem. Eng. Asp. (2020). https://doi.org/10.1016/j.colsurfa.2020.124643
46. X. Yuan, J. Li, L. Luo, Z. Zhong, X. Xie, Advances in sorptive removal of hexavalent chromium (Cr(VI)) in aqueous solutions using polymeric materials. Polymers **15**(2), 388–421 (2023). https://doi.org/10.3390/polym15020388
47. Q. Zhou, J. Huang, X. Zhang, Y. Gao, Assembling polypyrrole coated sepiolite fiber as efficient particle adsorbent for chromium (VI) removal with the feature of convenient recycling. Appl. Clay Sci. **166**, 307–317 (2018). https://doi.org/10.1016/j.clay.2018.09.031
48. L.Y. Li, G. Cao, R.S. Zhu, Adsorption of Cr(VI) from aqueous solution by a litchi shell-based adsorbent. Environ. Res. **196**, 110356 (2021). https://doi.org/10.1016/j.envres.2020.110356
49. A. Hosseinkhani, B. Forouzesh Rad, M. Baghdadi, Efficient removal of hexavalent chromium from electroplating wastewater using polypyrrole coated on cellulose sulfate fibers. J. Environ. Manag. **274**, 111153 (2020). https://doi.org/10.1016/j.jenvman.2020.111153
50. H. Wang, X.Z. Yuan, Y. Wu, X.H. Chen, L.J. Leng, H. Wang, H. Li, G.M. Zeng, Facile synthesis of polypyrrole decorated reduced graphene oxide–$Fe_3O_4$ magnetic composites and its application for the Cr(VI) removal. Chem. Eng. J. **262**, 597–606 (2015). https://doi.org/10.1016/j.cej.2014.10.020
51. J.W. Gao, G. Li, Y.F. Yao, J.M. Jiang, Preparation and characterization of montmorillonite/polypyrrole nanocomposites by in-situ chemical polymerization. J. Macromol. Sci. B Phys. **50**(7), 1364–1375 (2011). https://doi.org/10.1080/00222348.2010.497688
52. D.M. Liu, C. Dong, B.J. Xu, Preparation of magnetic kaolin embedded chitosan beads for efficient removal of hexavalent chromium from aqueous solution. J. Environ. Chem. Eng. **9**(4), 105438 (2021). https://doi.org/10.1016/j.jece.2021.105438
53. Y. Li, Y.P. Wang, X.Q. Liu, S. Wang, X.L. Jing, Facilely prepared conductive hydrogels based on polypyrrole nanotubes.

Chem. Pap. **75**(10), 5113–5120 (2021). https://doi.org/10.1007/s11696-021-01559-1
54. Y. An, X. Zhang, X. Wang, Z. Chen, X. Wu, Nano@lignocellulose intercalated montmorillonite as adsorbent for effective Mn(II) removal from aqueous solution. Sci. Rep. **8**(1), 10863 (2018). https://doi.org/10.1038/s41598-018-29210-2
55. K. Roy, P. Mondal, S.P. Bayen, P. Chowdhury, Sonochemical synthesis of polypyrrole salt and study of its Cr(VI) sorption-desorption properties. J. Macromol. Sci. A **49**(11), 931–935 (2012). https://doi.org/10.1080/10601325.2012.722852
56. L. Xiang, C.G. Niu, N. Tang, X.X. Lv, H. Guo, Z.W. Li, H.Y. Liu, L.S. Lin, Y.Y. Yang, C. Liang, Polypyrrole coated molybdenum disulfide composites as adsorbent for enhanced removal of Cr(VI) in aqueous solutions by adsorption combined with reduction. Chem. Eng. J. **408**(15), 127281 (2021). https://doi.org/10.1016/j.cej.2020.127281
57. A.A. Rouhaninezhad, S. Hojati, M.N. Masir, Adsorption of Cr(VI) onto micro- and nanoparticles of palygorskite in aqueous solutions: effects of pH and humic acid. Ecotoxicol. Environ. Saf. **206**, 111247 (2020). https://doi.org/10.1016/j.ecoenv.2020.111247
58. Y.S. Ho, G. McKay, Kinetic models for the sorption of dye from aqueous solution by wood. Process. Saf. Environ. Prot. **76**(2), 183–191 (1998). https://doi.org/10.1205/095758298529326
59. X.M. Chen, W.G. Zhang, X.L. Luo, F. Zhao, Y.X. Li, R.H. Li, Z.H. Li, Efficient removal and environmentally benign detoxification of Cr(VI) in aqueous solutions by Zr(IV) cross-linking chitosan magnetic microspheres. Chemosphere **185**, 991–1000 (2017). https://doi.org/10.1016/j.chemosphere.2017.07.113
60. M. Chen, Q. Guo, J. Cui, W. Lv, Y. Yao, Enhanced sorption and reduction of Cr(VI) by the flowerlike nanocomposites combined with molybdenum disulphide and polypyrrole. Environ. Technol. **43**(18), 2796–2808 (2022). https://doi.org/10.1080/09593330.2021.1903566
61. Z. Hu, L. Wang, M. Liu, Z. Huang, J. Yang, W. Rao, H. Wang, Y. Xie, C. Yu, Preparation of MES@$Fe_3O_4$@$SiO_2$-PPy magnetic microspheres for the highly efficient removal of Cr(VI). New J. Chem. **46**(42), 20160–20171 (2022). https://doi.org/10.1039/d2nj04456k
62 I. Langmuir, The constitution and fundamental properties of solids and liquids. Part I. Solids. J. Am. Chem. Soc. **38**(11), 2221–2295 (1916). https://doi.org/10.1021/ja02268a002
63. H.M.F. Freundlich, Over the adsorption in solution. J. Phys. Chem. **57**, 1100–1107 (1906)
64. W.H. Sun, W.B. Zhang, H.L. Li, Q. Su, P. Zhang, L.H. Chen, Insight into the synergistic effect on adsorption for Cr(VI) by a polypyrrole-based composite. RSC Adv. **10**(15), 8790–8799 (2020). https://doi.org/10.1039/c9ra08756g
65. S. Sahu, P. Kar, N. Bishoyi, L. Mallik, R.K. Patel, Synthesis of polypyrrole-modified layered double hydroxides for efficient removal of Cr(VI). J. Chem. Eng. Data **64**(10), 4357–4368 (2019). https://doi.org/10.1021/acs.jced.9b00444
66. D. Yang, Y. Chen, J. Li, Y.F. Li, W. Song, X.G. Li, L.G. Yan, Synthesis of calcium-aluminum-layered double hydroxide and a polypyrrole decorated product for efficient removal of high concentrations of aqueous hexavalent chromium. J. Colloid Interface Sci. **607**(Pt 2), 1963–1972 (2022). https://doi.org/10.1016/j.jcis.2021.10.014
67. N.S. Alsaiari, A. Amari, K.M. Katubi, F.M. Alzahrani, F.B. Rebah, M.A. Tahoon, Innovative magnetite based polymeric nanocomposite for simultaneous removal of methyl orange and hexavalent chromium from water. Processes **9**(4), 576–591 (2021). https://doi.org/10.3390/pr9040576
68. A.S. Al-Wasidi, Y.G. Abouelreash, S. AlReshaidan, A.M. Naglah, Application of novel modified chitosan hydrogel composite for the efficient removal of eriochrome black T and methylene blue dyes from aqueous media. J. Inorg. Organomet. Polym. Mater. **32**(3), 1142–1158 (2022). https://doi.org/10.1007/s10904-021-02168-x
69. J.B. Yang, B. Huang, M.Z. Lin, Adsorption of hexavalent chromium from aqueous solution by a chitosan/bentonite composite: isotherm, kinetics, and thermodynamics studies. J. Chem. Eng. Data **65**(5), 2751–2763 (2020). https://doi.org/10.1021/acs.jced.0c00085
70. L. Song, F. Liu, C. Zhu, A. Li, Facile one-step fabrication of carboxymethyl cellulose based hydrogel for highly efficient removal of Cr(VI) under mild acidic condition. Chem. Eng. J. **369**, 641–651 (2019). https://doi.org/10.1016/j.cej.2019.03.126
71. X.X. Jia, Y.Q. Zhang, Z. He, F.Q. Chang, H.C. Zhang, T. Wågberg, G.Z. Hu, Mesopore-rich badam-shell biochar for efficient adsorption of Cr(VI) from aqueous solution. J. Environ. Chem. Eng. **9**(4), 105634 (2021). https://doi.org/10.1016/j.jece.2021.105634
72. M. Bhaumik, A. Maity, V.V. Srinivasu, M.S. Onyango, Enhanced removal of Cr(VI) from aqueous solution using polypyrrole/$Fe_3O_4$ magnetic nanocomposite. J. Hazard. Mater. **190**(1–3), 381–390 (2011). https://doi.org/10.1016/j.jhazmat.2011.03.062
73. C. Lei, C.W. Wang, W.Q. Chen, M.H. He, B.B. Huang, Polyaniline@magnetic chitosan nanomaterials for highly efficient simultaneous adsorption and in-situ chemical reduction of hexavalent chromium: removal efficacy and mechanisms. Sci. Total Environ. **733**, 139316 (2020). https://doi.org/10.1016/j.scitotenv.2020.139316
74. E.T. Kang, Y.P. Ting, K.L. Tan, Electroless reduction and precipitation of gold from acid solution by polypyrrole. J. Appl. Polym. Sci. **53**(11), 1539–1545 (1994). https://doi.org/10.1002/app.1994.070531116